Dipolar Excitations at the L_{III} X-Ray Absorption Edges of the Heavy Rare-Earth Metals

S. D. Brown,[1,8] P. Strange,[2] L. Bouchenoire,[1,8] B. Zarychta,[3] P. B. J. Thompson,[1,8] D. Mannix,[1,8] S. J. Stockton,[3] M. Horne,[3] E. Arola,[3,4] H. Ebert,[5] Z. Szotek,[6] W. M. Temmerman,[6] and D. Fort[7]

[1]*XMaS, European Synchrotron Radiation Facility, B.P. 220, 38043 Grenoble Cedex, France*
[2]*School of Physical Sciences, University of Kent, Canterbury, Kent CT2 7NH, United Kingom*
[3]*Keele University, Keele, Staffordshire ST5 5BG, United Kingdom*
[4]*Optoelectronics Research Centre, Tampere University of Technology, P.O. Box 692, FIN-33101 Tampere, Finland*
[5]*Department Chemie/Physikalische Chemie, Universität München, Butenandtstrasse 5-13, D-81377 Munich, Germany*
[6]*Daresbury Laboratory, Daresbury, Warrington WA4 4AD, United Kingdom*
[7]*The University of Birmingham, Edgbaston, Birmingham B15 2TT, United Kingdom*
[8]*Liverpool University, Liverpool L69 3BX, United Kingdom*

(Received 15 December 2006; published 13 December 2007)

We report measured dipolar asymmetry ratios at the L_{III} edges of the heavy rare-earth metals. The results are compared with a first-principles calculation and excellent agreement is found. A simple model of the scattering is developed, enabling us to reinterpret the resonant x-ray scattering in these materials and to identify the peaks in the asymmetry ratios with features in the spin and orbital moment densities.

DOI: 10.1103/PhysRevLett.99.247401 PACS numbers: 78.70.Ck, 61.10.Dp, 78.70.En

The interpretation of magnetic x-ray spectroscopies at the L absorption edges of rare-earth materials has been a subject of long-standing controversy. Spectra consist of two main features: a large peak at an energy close to the absorption white-line (feature A), interpreted as arising from dipolar ($E1$) transitions coupling $2p$ core levels to unoccupied $5d$ and $6s$ states, and a smaller peak a few eV lower (feature B), attributed to quadrupolar ($E2$) transitions coupling the same core levels to unoccupied $4f$ states [1–6]. In this Letter we reexamine the dipolar or quadrupolar character of these structures.

X-ray resonant magnetic scattering (XRMS) assigns the $E1$ or $E2$ nature of spectral features through analysis of the scattered x-ray polarization [7,8] and comparison with theory [9–11]. Resonant inelastic x-ray scattering assigns the $E1$ or $E2$ nature from their relative energy positions [5,6]. In x-ray magnetic circular dichroism (XMCD) assignment is achieved by modeling variations in signal with the angle between the incident x-ray polarization and the magnetization direction [12]. However, problems arise in the sign of signals and the relative importance of $E2$ ''contamination.'' Spectra show dispersive shapes which are thought to arise from exchange splitting and matrix element effects [13,14].

In this Letter we report combined experimental and theoretical investigations of x-ray resonant interference scattering (XRIS) in the ferro- or ferrimagnetic phases of heavy rare earths. For the heavy rare-earth hexagonal crystal structures, $E1 - E2/M1$ scattering is allowed and may contribute to asymmetry ratios. We exploit the possibility of virtually turning off the $E2$ signal by scattering horizontally through angles close to 90°, thus isolating $E1$ scattering. To investigate this further, first-principles calculations were performed for pure $E1$, pure $E2$, and total ($E1$ and $E2$) scattering in this geometry. The $E1 - E2$ contributions were found to be 2 orders of magnitude smaller than the pure $E1$ scattering and thus can be eliminated as key contributions. We show that feature B is in fact of mixed $E1$ and $E2$ origin in both absorption and scattering spectra and that the $E1$ contribution is substantial. Using both first-principles scattering theory (FPST) and an atomiclike model, we reproduce features A and B and thus confirm the $E1$ nature of our spectra. This has enabled identification of strong antiparallel hybridization between the unoccupied $4f$ and $5d$ spin moments, which provides a natural explanation for the size and dispersive line shape observed in XMCD. A direct hybridization between f and d states with parallel orbital moments is also identified. A changeover from magnetism dominated by f-d exchange and spin to magnetism dominated by spin-orbit coupling (SOC) and orbital $4f$ and $5d$ magnetizations occurs around Er. However, with both the FPST and the model, the Tm XRIS spectra were found to be inverted with respect to the experimental data. Examining this discrepancy suggests the possibility that in the excited state, the $4f$ SOC might differ from that of the Hund's rules ground state configuration, although we stress that assignment of an $E1$ contribution to feature B is independent of this possibility.

The experiments were performed at the XMaS beamline BM28 at the European Synchrotron Radiation Facility [15]. Ferri/ferromagnetic charge-magnetic XRIS measurements were performed monitoring (300) reflections from each element, while scattering horizontally through angles of about 90° at their L_{III} edges. Data were obtained through reversal of a vertical magnetic field applied along the c axis at each point of energy scans, resulting in field-dependent spectra, an example of which is given in the top panel of Fig. 1 for Gd. It is usual to present such data as an asymmetry ratio, R, as defined in Eq. (3) [16]. Spectra were calculated from a fully relativistic FPST of XRMS [17,18]. The electronic structure of the elements was

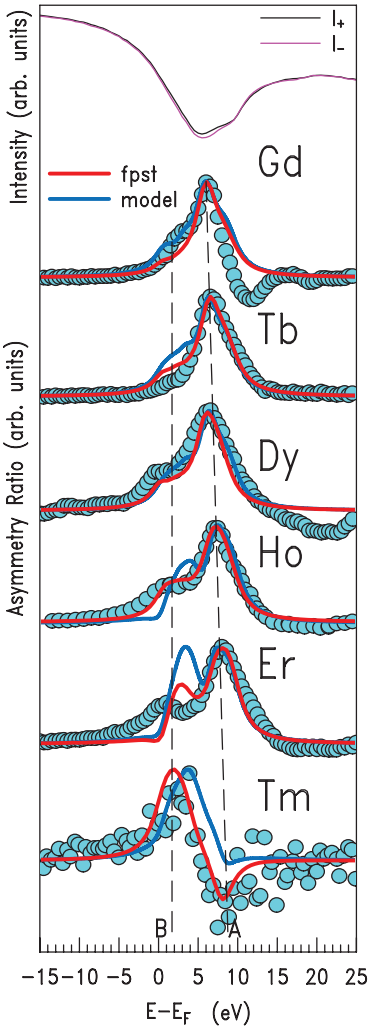

FIG. 1 (color). Top curves, field-dependent energy scan for Gd. At each energy point the field was reversed many times and averaged to reduce systematic errors. Below, charge-magnetic XRIS asymmetry ratios [see Eq. (3)]. Experimental data (cyan), first-principles x-ray scattering theory (red) and model (blue). Statistical errors are smaller than the plotted points. In Tm (with scattering angle $<90°$), the asymmetry ratio reverses sign. Therefore we have simply inverted the curves for Tm in the figure. The curves consist of a dominant high energy peak and a lower energy shoulder that becomes more pronounced with increasing atomic number. The higher energy peak results from scattering off the spin moment and the lower energy peak arises from scattering from both the spin and orbital moments. The changing relative size and position of these peaks reflects the change in relative magnitude of these quantities. The zero of energy here is the L_{III} edge which we equate to the Fermi energy.

found using the fully relativistic SIC-LMTO method [19,20].

To model the XRIS spectra, we write the total $E1$ scattering amplitude as a sum of amplitudes due to charge scattering (subscript 0) and spin (subscript S) and orbital (subscript L) magnetic scattering:

$$f_{E1}(E) = -\left(\frac{3}{4\pi q}\right)\{\cos(2\theta)(F_0' + iF_0'') + i\mathbf{m}\sin(2\theta)(F_S' + iF_S'' + F_L' + iF_L'')\}, \quad (1)$$

where single (double) primes indicate the real (imaginary) part of the resonant scattering amplitudes F and $\mathbf{m}$ is a unit vector in the magnetization direction. On reversal of the magnetization, magnetic terms in Eq. (1) change sign while the charge terms do not. The absorption coefficient is directly proportional to the density of states (DOS). In turn the Optical Theorem [21] states that the absorption coefficient is directly proportional to the imaginary part of the forward scattering amplitude. We therefore replace the imaginary parts of the scattering amplitudes of Eq. (1) with the equivalent DOS found from the electronic structure calculations and their real parts with a Kramers-Kronig transformation [22] of these quantities. This method ignores matrix element effects which we have found to be slowly varying over the energy range of interest. It also implies that the extra transparency this model yields will lead to only a small accuracy loss. We define [10]

$$\hat{\rho}_0 = \hat{\rho}_\uparrow + \hat{\rho}_\downarrow, \quad \text{and} \quad \hat{\rho}_S = \frac{1}{2}(\hat{\rho}_\uparrow - \hat{\rho}_\downarrow) \quad (2)$$

as the charge and spin-polarized convoluted densities of states, respectively, where $\hat{\rho}\uparrow(\downarrow)$ is the spin up (down) unoccupied DOS convoluted with a Lorentzian (here, and in the FPST, of width 3 eV for all elements) representing the core hole lifetime. Replacing the scattering amplitudes in Eq. (1) with the appropriate unoccupied DOS we arrive at

$$R = \frac{I_+ - I_-}{I_+ + I_-} = \frac{2\tan 2\theta\{2P_S(\hat{\rho}_\downarrow\hat{\rho}_\uparrow'' - \hat{\rho}_\uparrow\hat{\rho}_\downarrow'') + P_L(\hat{\rho}_0\hat{\rho}_L'' - \hat{\rho}_0''\hat{\rho}_L)\}}{\hat{\rho}_0''^2 + \hat{\rho}_0^2}, \quad (3)$$

where I_+ is the cross section for the magnetization in one direction and I_- is for it reversed; the $\hat{\rho}''$s represent the Kramers-Kronig transformations of the DOS. P_S and P_L are the same photoelectron spin and orbital polarizations adopted in the analysis of XMCD and we have taken the simple values $|P_S| = 1/4$ and $|P_L| = 3/4$. Our theoretical and experimental approach of measuring photon scattering has significant advantage over first order methods (absorption, emission): (i) the XRIS asymmetry ratio is enhanced by a factor of $2\tan(2\theta)$, leading to easily measurable signals; (ii) diffraction is a highly efficient scattering mechanism leading to enhancement of the signal-to-noise ratio; (iii) we reference the signs of both the spin and the orbital contributions (and their real parts) to those of the charge, which enhances sensitivity; (iv) polarization dependence allows almost complete separation of $E1$ and $E2$ events. Finally, in contrast to antiferromagnetic XRMS, no absorption correction is required.

Figure 1 shows measured XRIS asymmetry ratios at the L_{III} edges. The spectra resemble resonant inelastic x-ray scattering spectra in [6], where the low energy feature was designated as $E2$ from its energy position. Also shown are pure $E1$ results of the FPST and model. The experimental results have been rigidly shifted to superpose the high energy peaks with those in the calculated spectra and rescaled. In all elements the data contain an $E1$ peak, feature A, with a lower energy $E1$ shoulder or peak, feature B. For Tm, Feature A has become inverted; moreover, for the Hund's rules ground state $4f$ electronic configuration ($J = L + S$), both the FPST and the model give a negative peak at low energy and a positive peak at high energy. Er also shows a dispersive line-shape for the $J = L + S$ $4f$ configuration. Small improvements in agreement between experiment and both calculations are observed for the $J = |L - S|$ $4f$ configuration for all elements. Therefore we show the non-Hund's rules compliant results, although we note that for Gd to Ho this makes very little difference and that even for Er and Tm, features A and B still occur at the same energies as those observed with the Hund's rules configuration.

The $E2$ scattering amplitude simplifies in the adopted geometry; just one reversible magnetic term remains. The total $E1 + E2$ asymmetry ratio leads to pure $E1$, pure $E2$, and mixed $E1E2$ charge-magnetic interference terms. $E2$ charge scattering events are 2 orders of magnitude smaller than $E1$ charge scattering events. However, this is not true for $E2$ magnetic scattering, which is enhanced relative to $E1$ magnetic scattering, due to the large $4f$ and small $5d$ moments. This yields asymmetry ratios where the $E1$ charge-$E2$ magnetic term is scaled by a factor $\cos(2\theta)$ relative to pure $E1$ terms. Thus for Ho, Er, and Tm ($2\theta = 96.1°$, $93.3°$, and $89.5°$) the $E2$ contributions are reduced by factors of 0.10, 0.06, and 0.01, respectively. For Gd, Tb, and Dy the scattering angles exceed 100° and the $E2$ suppression is less efficient. Clearly both the FPST and the model predict $E1$ scattering at energy position B for these elements, which fits the experimental data. We have performed polarization analysis in the antiferromagnetic phases of Tb to Tm, which reveals almost pure E1 scattering in Ho, Er, and Tm and sets an upper limit of the $E2$ contribution in Tb and Dy of a few percent [16].

The Hund's rules ground state calculations give total magnetic moments in fair agreement with measured values for Gd to Tm. Exchange splitting dominates for Gd to Ho, after which SOC leads to bunching of mixed spin up or down states around the energies of the Lu $j = 5/2$ and $7/2$ closed shell configuration. This is seen in the exchange splitting between occupied $5d$ spin states, which decreases from 0.63 eV in Gd to 0.04 eV in Tm. The occupied $5d$ spin moment ($0.292\mu_B$ in Gd, $0.023\mu B$ in Er, and $-0.026\mu_B$ in Tm) is aligned with that of the $4f$s for Gd to Er but is antiparallel for Tm. They exhibit dispersive line shapes, as seen in Fig. 2(a). The positive parts of the dispersive shapes are stationary at around 1 eV above the Fermi energy for all elements. These features coincide with negative peaks in

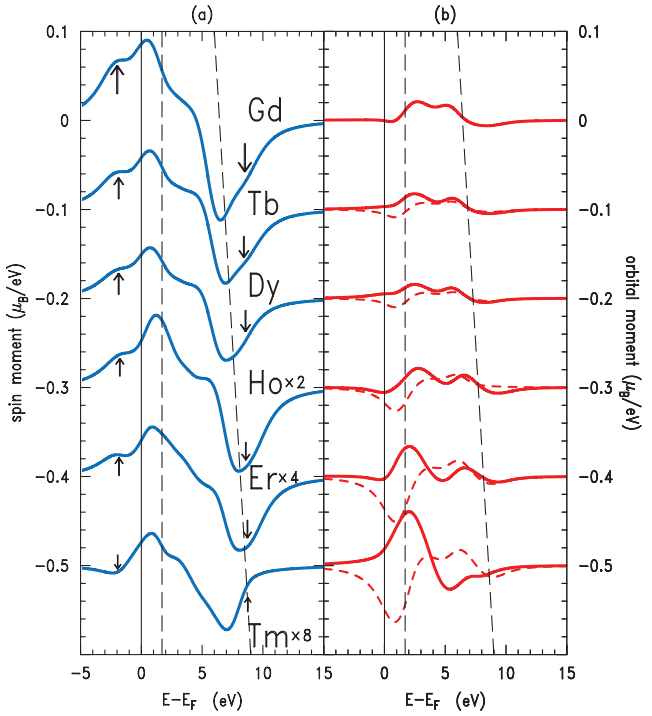

FIG. 2 (color). (a) Spin-polarized convoluted $5d$ DOS: Beyond Gd, the data are offset by $-0.1\mu_B$/eV with respect to the preceding element. The DOS have been convoluted with 3 eV wide Lorentzians to represent core hole broadening. The center of the occupied $5d$ spin moments is also shown below E_F, indicated by the arrows. The arrows above E_f show the energy of the center of the $5d$ spin moment closure peaks. The near vertical dashed lines mark the position of features A and B in Fig. 1. (b) Orbital polarized convoluted $5d$ DOS: Data are scaled and offset as in (a). The dashed line represents the Hund's rule state and the full line is for the non-Hund's rule state.

the unoccupied $4f$ spin moments, shifted to slightly higher energy due to the large increase in available d states from 0 to 1 eV. The negative parts of the dispersive shapes occur at higher energies, ~6.5 eV for Gd, increasing to ~8 eV for Er, reducing to 7 eV for Tm. The stationary nature of the low energy peaks leads us to conclude that they arise from antiparallel f-d spin hybridization. This large positive contribution to the $5d$ unoccupied moment must be compensated, and this is the origin of the large negative part of the dispersive oscillation at high energy. In Tm, where the occupied d moment is reversed relative to that of the $4f$ states, this feature changes in a positive sense, as indicated by the arrows in Fig. 2(a). This is also reflected in the polarity of feature A in Fig. 1. We also find that the $6s$ unoccupied spin moment does not exhibit the same dispersive shape as the $5d$s. The parts of the unoccupied $6s$ spin states which negatively reflect the occupied moments are hybridized with the $5d$ DOS in the high energy tails of the $5d$ band. Clearly, this large $4f$ induced oscillation must be the origin of the dispersive XMCD spectra. Even if there were no d-band polarization, this dispersive feature would be present, though its integral would be zero. In common

with Kim *et al.* [14] we observe an increase in the size of the matrix elements as energy increases.

The $5d$ orbital moments are shown in Fig. 2(b). They exhibit double peaks, split by about 4 eV, for all elements except Tm. Here, the centroids of the two peaks are aligned with the centers of the $5d$ bands, which are at 3.5 to 5 eV for Gd to Tm. This splitting is visible in the total $5d$ DOS and is also apparent in the unoccupied spin moment in Fig. 2(a). We conclude that this splitting is due to the crystal field (which is essentially unaffected by the partially filled f-shell configuration). In addition, there are negative dips in the Hund's rules spectra (dashed lines) which are also stationary, at around 1 eV above E_f for all elements. These features coincide with the negative peaks in the unoccupied $4f$ orbital moments, again, slightly shifted up in energy due to available d states. Further, if we reverse the sign of the $4f$ spin-orbit coupling (non-Hund's rules configuration, solid lines), these features change sign and are pulled down in energy along with the unoccupied $4f$ orbital moments. We conclude that these features are due to parallel f-d orbital hybridization. The higher energy $5d$ orbital moments are fairly independent of the $4f$ orbital configuration, as was concluded in [14]. For Er and Tm, however, the hybridized $4f$ orbital moments dominate over the crystal field splitting. Our results strongly suggest that in the presence of the $2p^{3/2}$ core hole, the $4f$ SOC differs from that of the Hund's rules ground state. It has been suggested [23] that in the presence of the core hole, the $4f$ levels pull down in energy by $\sim$3 eV (although earlier calculations found larger values [24]). As this also corresponds to calculated energy difference between the $J = L + S$ and $|L - S|$ $4f$ configurations, it is conceivable that the core hole energy might be taken up in a reconfiguration of the $4f$ states during the excitation, and our results support this scenario. Examination of the positions of features A and B in Fig. 2 reveals that feature A is of almost pure spin origin, whereas feature B is of mixed spin and orbital origin. The correlation of peaks A and B in Fig. 1, with structure in Fig. 2(a) and 2(b), demonstrates that the dipolar asymmetry ratios at the L_{III} edges reflect the progression from spin-dominated Gd to orbital-dominated Er and Tm electronic structure.

This work, with analogous work at the L_{II} edge, opens the way for quantitative measurements of quadrupole scattering contributions and the development of new sum rules.

We gratefully acknowledge the financial support of EPSRC. The experimental work was performed on the EPSRC-funded XMaS beamline at the ESRF, directed by M. J. Cooper and C. A. Lucas. S. D. B. would like to thank S. P. Collins, S. W. Lovesey, and staff of the ESRF, notably C. Detlefs, for stimulating discussions.

[1] G. Shutz, W. Wagner, W. Wilhelm, P. Kienle, R. Zeller, R. Frahm, and G. Materlik, Phys. Rev. Lett. **58**, 737 (1987).
[2] P. Fischer, G. Schutz, S. Stahler, and G. Weisinger, J. Appl. Phys. **69**, 6144 (1991).
[3] F. Baudelet, C. Giorgetti, S.Pizzini, C. H. Brouder, E. Dartyge, A. Fontaine, J. P. Kappler, and G. Krill, J. Electron Spectrosc. Relat. Phenom. **62**, 153 (1993).
[4] D. Gibbs, D. R. Harshman, E. D. Isaacs, D. B. McWhan, D. Mills, and C. Vettier, Phys. Rev. Lett. **61**, 1241 (1988).
[5] M. H. Krisch, C. C. Kao, F. Sette, W. A. Caliebe, K. Hamalainen, and J. B. Hastings, Phys. Rev. Lett. **74**, 4931 (1995).
[6] F. Bartolome, J. M. Tonnerre, L. Seve, D. Raoux, J. Chaboy, L. M. Garcia, M. Krisch, and C. C. Kao, Phys. Rev. Lett. **79**, 3775 (1997).
[7] D. Gibbs, G. Grubel, D. R. Harshman, E. D. Isaacs, D. B. McWhan, D. Mills, and C. Vettier, Phys. Rev. B **43**, 5663 (1991).
[8] C. Detlefs, A. H. M. Z. Islam, A. I. Goldman, C. Stassis, P. C. Cranfield, J. P. Hill, and D. Gibbs, Phys. Rev. B **55**, R680 (1997).
[9] M. Blume, J. Appl. Phys. **57**, 3615 (1985).
[10] S. W. Lovesey and S. P. Collins, *X-ray Scattering and Absorption by Magnetic Materials* (Oxford University Press, Oxford, 1996).
[11] J. P. Hill and D. F. McMorrow, Acta Crystallogr. Sect. A **52**, 236 (1996).
[12] J. C. Lang, G. Srajer, C. Detlefs, A. I. Goldman, H. Konig, W. Xindong, B. N. Harmon, and R. W. McCallum, Phys. Rev. Lett. **74**, 4935 (1995).
[13] M. van Veenendaal, J. B. Goedkoop, and B. T. Thole, Phys. Rev. Lett. **78**, 1162 (1997).
[14] J. W. Kim, Y. Lee, D. Wermeille, B. Sieve, L. Tan, S. L. Bud'ko, S. Law, P. C. Cranfield, B. N. Harmon, and A. I. Goldman, Phys. Rev. B **72**, 064403 (2005).
[15] S. D. Brown, L. Bouchenoire, D. Bowyer, J. Kervin, D. Laundy, M. J. Longfield, D. Mannix, D. F. Paul, A. Stunault, P. Thompson, M. J. Cooper, C. A. Lucas, and W. G. Stirling, J. Synchrotron Radiat. **8**, 1172 (2001).
[16] S. D. Brown, P. Strange, L. Bouchenoire, B. Zarychta, P. B. J. Thompson, D. Mannix, S. J. Stockton, M. Horne, E. Arola,H. Ebert, Z. Szotek, W. M. Temmerman, and D. Fort (to be published).
[17] E. Arola, P. Strange, and B. L. Gyorffy, Phys. Rev. B **55**, 472 (1997).
[18] E. Arola, M. Horne, P. Strange, H. Winter, Z. Szotek, and W. M. Temmerman, Phys. Rev. B **70**, 235127 (2004).
[19] W. M. Temmerman, A. Svane, Z. Szotek, and H. Winter, in *Electronic Density Functional Theory: Recent Progress and New Directions*, edited by J. F. Dobson, G. Vignale, and M. P. Das (Plenum, New York, 1997).
[20] S. V. Beiden, W. M. Temmerman, Z. Szotek, and G. A. Gehring, Phys. Rev. Lett. **79**, 3970 (1997).
[21] G. Baym, *Lectures on Quantum Mechanics* (Addison-Wesley, Reading, MA, 1990).
[22] C. Kittel, *Introduction to Solid State Physics* (John Wiley and Sons, New York, 1986).
[23] P. Carra, B. N. Harmon, B. T. Thole, M. Altarelli, and G. A. Sawatzky, Phys. Rev. Lett. **66**, 2495 (1991).
[24] J. F. Herbst and J. W. Wilkins, in *Handbook of the Physics and Chemistry of the Rare Earths* 10, 356 (1988) and references therein.